



## 3D limit analysis of masonry pavilion domes on octagonal drum subjected to vertical loads

C. Anselmi, F. Galizia

*University of Naples "Federico II", Department of Structures for Engineering and Architecture, Italy*  
anselmi@unina.it, fgalizia@unina.it

E. Sietta

*Sapienza University of Rome, Department of Structural and Geotechnical Engineering, Italy*  
e.sietta@virgilio.it

**ABSTRACT.** Within the framework of limit design applied to masonry structures, this paper aims at analyzing the different behavior of a pavilion dome according to the adopted construction and reinforcement technologies. By using the static theorem applied to the dome discretized in rigid macro-blocks of variable shape aligned along parallels and meridians, a mathematical model has been constructed in order to search for the load collapse multiplier, and thus to evaluate the degree of structural safety. Then, the associated failure mechanism is represented at the instant in which the collapse is reached. The program implementing the model is sufficiently versatile and, in addition to the mechanical characteristics, allows to define the intrados profile, the thickness variability, as well as to insert any window opening in the drum, the lantern at the top and the hoops at each level. The results shown here are concerned with some numerical applications carried out on a theoretical dome, as well as with a preliminary analysis of the dome of Santa Maria del Fiore in Florence by Brunelleschi.

**KEYWORDS.** Masonry; Dome on octagonal drum; Limit analysis; No-tension material; Yield surface.



**Citation:** Anselmi, C., Galizia, F., Sietta, E., 3D limit analysis of masonry pavilion domes on octagonal drum subjected to vertical loads, *Frattura ed Integrità Strutturale*, 51 (2020) 486-503.

**Received:** 26.06.2019

**Accepted:** 12.12.2019

**Published:** 01.01.2020

**Copyright:** © 2020 This is an open access article under the terms of the CC-BY 4.0, which permits unrestricted use, distribution, and reproduction in any medium, provided the original author and source are credited.

### INTRODUCTION

Within the framework of limit design applied to masonry structures, this paper aims at analyzing the different behavior of a pavilion dome according to the adopted construction and reinforcement technologies; for example, if in correspondence of the ribs the bricks of the contiguous sails are well interlocked (as in the Santa



Maria del Fiore dome) the dome shows a much greater load-bearing capacity compared to the case of interlocking between the bricks completely missing (Santa Maria dell'Umiltà dome in Pistoia).

In several previous works [1, 2, 3, 4] the authors had already dealt with rotation domes subject to vertical and horizontal loads; by using the static theorem of the limit analysis applied to the dome discretized in rigid macro-blocks of variable shape aligned along the parallels and the meridians, several optimization models have been implemented in order to search for the load collapse multiplier, thus to evaluate the degree of structural safety.

It should be noted that many different modelling approaches in the literature were used to investigate the behaviour of masonry constructions, and particularly of domes. Among those, it is worth mentioning the works by O'Dwyers on the funicular analysis of masonry vaults [5], and those using analytical and finite element models [6, 7, 8, 10, 11, 12]. Rigid block models based on limit analysis and contact dynamics were also adopted [9, 13].

In the previously papers, as in this, the yield domain conditions for the quadrilateral interfaces between the macro-blocks are expressed in terms of stress resultants, in observance of the following mechanical assumptions: inability to carry tension, unlimited or limited compressive strength (in the second case the domain is suitably linearized), frictional sliding with dilatancy. This last hypothesis, even if not realistic, has been assumed because in some cases the influence of failure for sliding is negligible in the kinematic mechanism of the domes; that allows us to base the formulation on simple optimization problems rather than more involved nonlinear analyses, with considerable reduction of computational costs.

The yield domain conditions for the quadrilateral interfaces between the macro-blocks are expressed in terms of stress resultants, in observance of the following mechanical assumptions: inability to carry tension, unlimited or limited compressive strength (in the second case the domain is suitably linearized), frictional sliding with dilatancy. This last hypothesis, even if not realistic, has been assumed because in some cases the influence of sliding failure is negligible in the kinematic mechanism of the domes; that allows us to base the formulation on simple optimization problems rather than more involved nonlinear analyses, with considerable reduction of computational costs.

It should be pointed out that the sliding failure was taken into account assuming a friction coefficient  $f_c = 0.75$ . This value is perhaps excessive when compared with those taken by other authors in the most recent literature [14, 15, 16, 17] where, for different materials, coefficients varying from 0.63 to 0.69 are used. However, even when a value included into that range is taken into account, the results - static and kinematic - are almost identical to those which are here presented (at least for the tested cases 7 and 11 of Tab. 1). Furthermore, analyzing the response even in the case of a further reduction in the friction coefficient, it was found that the result remains unchanged up to the value  $f_c = 0.2 - 0.22$  for which the value of the collapse multiplier decreases and the kinematic mechanism shows an evident failure for sliding. Finally, for  $f_c = 0.18 - 0.20$  there is a further reduction of the multiplier, but the collapse mechanism is qualitatively equivalent.

Compared to previous tackled problems, in this work there are two new aspects: a different type of dome, because it is set on octagonal and not circular drum, and the role played by the interlocking between the bricks in correspondence of the ribs on the bearing capacity of the dome.

As we consider vertical loads, we studied a dome segment - corresponding to one sixteenth - between two contiguous meridian symmetry planes (Fig. 1). In this context, we have developed a program through Excel and its Solver to solve the static optimization problem that provides the collapse multiplier. Once the collapse multiplier has been defined, again using Excel, the corresponding kinematic problem is implemented to represent the failure mechanism at the instant in which the collapse is reached. In order to simulate the lack of interlocking between the bricks at the ribs or its presence, an advantageous aspect in the present modeling is that the yield conditions on the related interfaces of the macro-blocks can be either introduced (the failure is possible) or not (the failure is not possible).

Although for the considered application cases has always been used a discretization in only eight macro-elements (six for the dome and two for the drum), the program implemented in Excel appears sufficiently versatile and, in addition to the mechanical characteristics, allows to define the intrados profile, the thickness variability, as well as to insert any window opening in the drum, the lantern at the top and the hoops at each level. Some results of application cases are shown and, finally, a first approach was made to the analysis of the Santa Maria del Fiore dome in Florence, built by Brunelleschi.

Of course, models with reduced block dimensions could be implemented to take into account failure mechanisms which were not considered in the present work. However, it should be noted that the configuration of the macro-blocks taken into consideration aimed at reproducing the main features of the crack patterns which are frequently observed on masonry domes, such as those investigated in this manuscript. As the authors pointed out in the manuscript, such crack patterns usually involve the ribs and the webs along radial and meridian interfaces which correspond to the ones considered in the model that was presented. However, it is clear that further analysis could be carried out to investigate the effect of interlocking and block size on the obtained failure mechanism.



## PRELIMINARY AND GEOMETRIC FEATURES

Since only vertical loads are considered, a dome segment has been studied - corresponding to a sixteenth - between two contiguous meridian planes of symmetry, one passing through the center line of a sail, the other for a rib (Fig.1a). In the horizontal section of the dome, the angle between the two symmetry planes is  $\pi/8$ , and the segment can be studied - at least in this first approach - as fixed at the drum base and subject to dead loads due to their own weight and live loads corresponding to increasing overloads, as well as to the actions on the interfaces belonging to the symmetry planes, which are the redundant unknowns of the static problem.

With regard to a dome segment of amplitude  $\varphi = \pi/8$  (Fig. 1b), a discretization in rigid blocks is made, each one bounded by two consecutive cross-sections  $i$  and  $i+1$  defined by the angles  $\theta_i$  and  $\theta_{i+1}$  respectively with the dome's Z-axis (Fig. 1c).

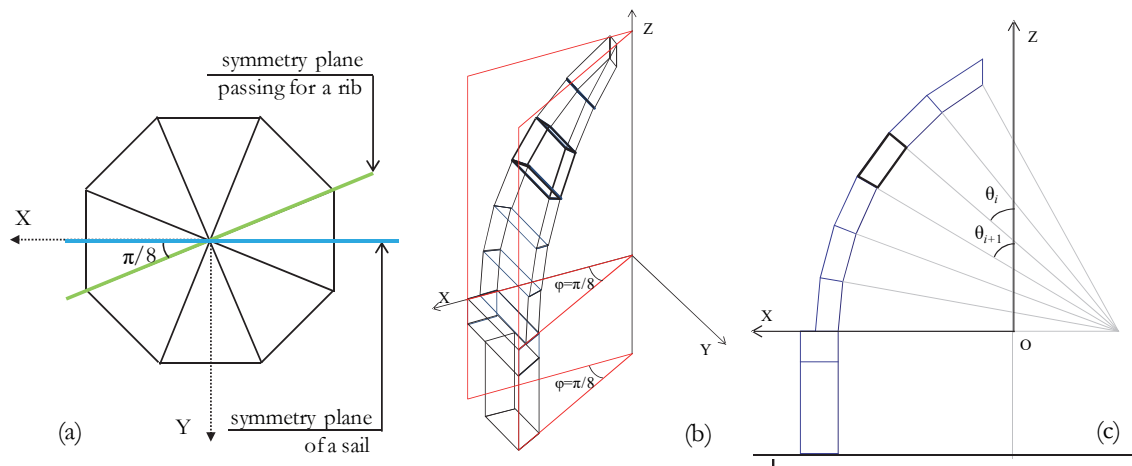


Figure 1: The dome segment. (a) the two contiguous meridian symmetry planes; (b) 3D view; (c) section in the X-Z plane.

The generic block like this defined have six faces: two of them - named *radial* - lying on the aforesaid radial cross-sections  $i$  and  $i+1$ , two other - named *meridian* - lying on meridian symmetry planes, and finally two other again lying on the extrados and intrados surfaces of dome respectively (Fig. 2).

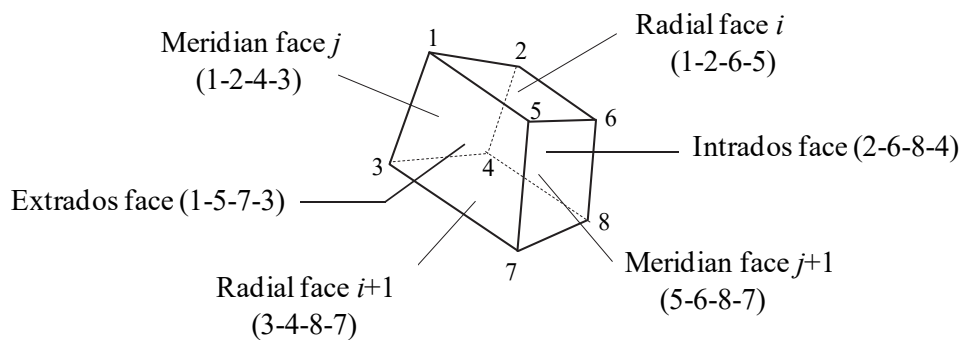


Figure 2: The generic block

Have been used two reference: the fixed one (O, X, Y, Z), to define the vertices coordinates of generic block (Fig.1), and a local one ( $G_f, n, r, t$ ) placed in  $G_f$  centroid of each contact interface with a contiguous block (Fig.3a), to define the stress resultants interacting through this generic interface, as shown below.

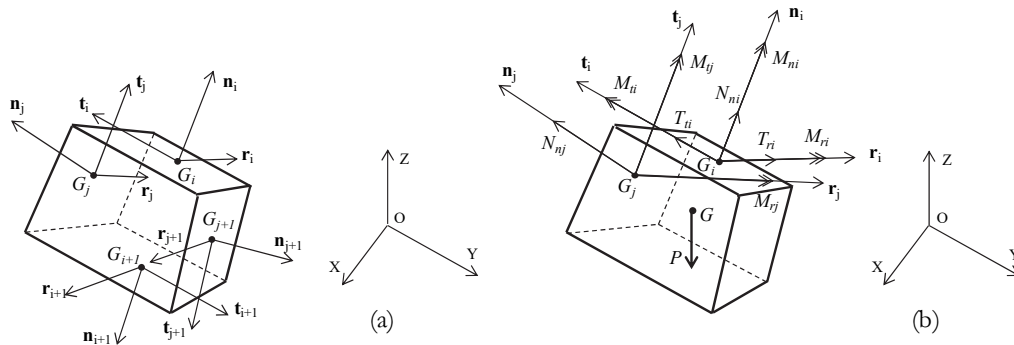


Figure 3: (a) Fixed and local references; (b) Own weight  $P$  acting in the  $G$  centroid of block and stress resultants applied on the  $i$  radial face and on  $j$  meridian face.

### FORCES ACTING ON THE SINGLE BLOCK

With reference to Fig. 3b, the generic block is subjected to the own weight  $P$  applied on its center of gravity  $G$ , and to the stress resultants applied on the centroid of each contact interface with a contiguous block, referred to the local reference  $n$ ,  $r$  and  $t$ .

The resultants on the radial interfaces are six, named normal force  $N_n$  (or simply  $N$ ), shear forces  $T_t$  and  $T_r$ , twist moment  $M_n$ , bending moments  $M_t$  and  $M_r$ , respectively applied on the interfaces  $i$  and  $i+1$ . Whereas, on the meridian interfaces  $j$  and  $j+1$ , lying on symmetry planes, the resultants are only three: the normal force  $N_n$  and the two bending moments  $M_t$  and  $M_r$ .

With reference to  $i$  and  $j$  interfaces, all these forces can be expressed in matrix form by the  $\mathbf{S}_i$  and  $\mathbf{S}_j$  vector respectively:

$$\mathbf{S}_i = \begin{bmatrix} \mathbf{R}_i \\ \mathbf{M}_i \end{bmatrix} = \begin{bmatrix} N_{ni} \\ T_{ti} \\ T_{ri} \\ M_{ni} \\ M_{ti} \\ M_{ri} \end{bmatrix}$$

$$\mathbf{S}_j = \begin{bmatrix} \mathbf{R}_j \\ \mathbf{M}_j \end{bmatrix} = \begin{bmatrix} N_{nj} \\ M_{tj} \\ M_{rj} \end{bmatrix}$$

Besides, must be consider the overload acting on the dome - named  $OL$  - understood as a covering load applied in the centroid of extrados face (see Fig. 2), that in the present formulation increases through a collapse multiplier  $\alpha$  (Fig. 4a).

If a lantern is present at the top of dome, also a force  $PL$  corresponding to one sixteenth of the lantern own weight will act on the block top (Fig. 4b), together with the  $OLL$  overload related to the small dome of the lantern (also increasing through the  $\alpha$  multiplier).

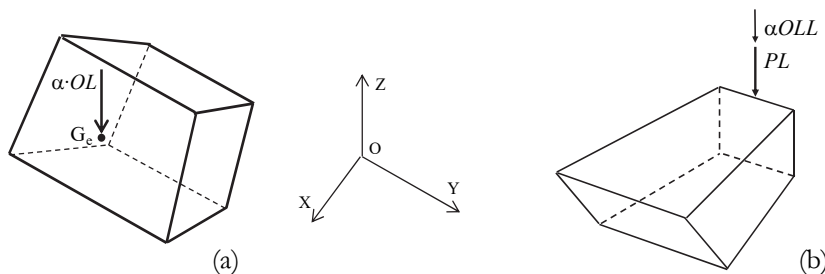


Figure 4: (a) The overload acting on the dome, increasing through an  $\alpha$  multiplier; (b) The force on the block on top corresponding to one sixteenth of the lantern own weight, together with the overload (which also increases through  $\alpha$ ) acting to the small dome of the lantern.

Finally, if hoops are inserted, the possible action of them is represented by a  $F_h$  force applied on extrados face, lying in a plane parallel to the dome springing and oriented towards the inside. Having fixed a suitable  $N_h$  pretension effort, the resultant force  $F_h = N_h \cdot \tan(\pi/8)$  is positioned at half the height with respect to the height of the generic parallel ring with hoop (point C in Fig. 5).

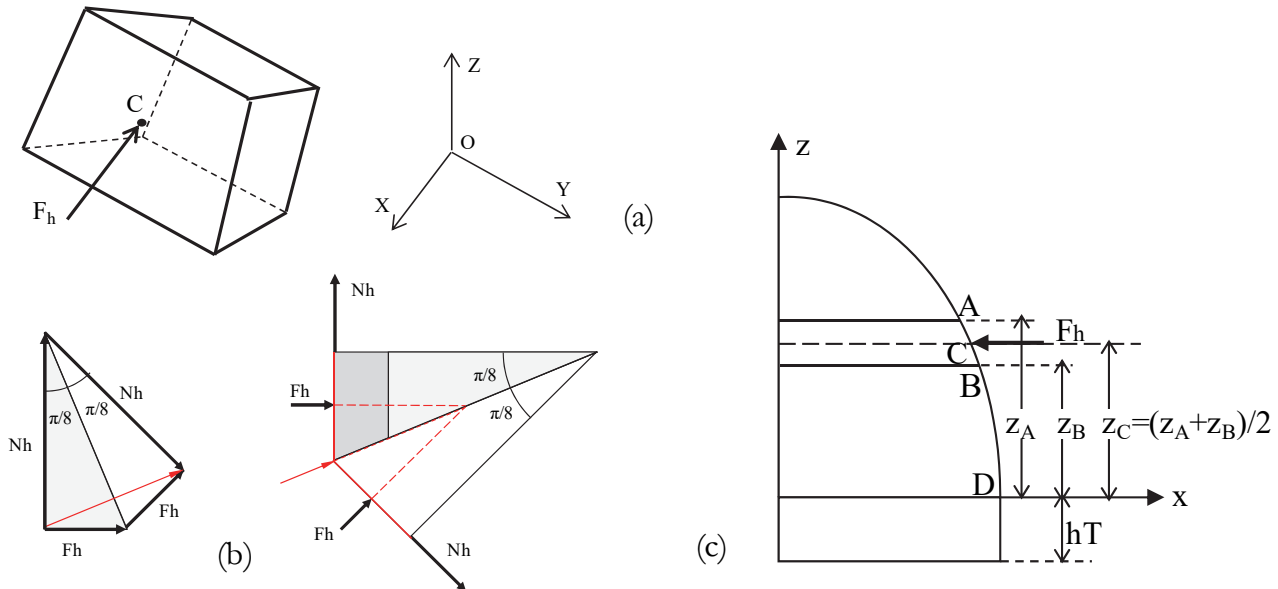


Figure 5: Force depending by the hoop. (a) The resultant force  $F_h$ ; (b)  $N_h$  pretension effort and  $F_h$  resultant force; (c) Level of C application point of  $F_h$  force.

## EQUILIBRIUM CONDITIONS FOR THE SINGLE BLOCK

The equilibrium conditions for the generic block, in the global reference frame  $X$ ,  $Y$  and  $Z$  are so formulated:

$$\mathbf{A}^e \mathbf{X}^e + \mathbf{B}^e \mathbf{Y}^e + \mathbf{C}^e \mathbf{S}_0^e + \mathbf{D}^e \mathbf{S}_1^e + \mathbf{F}_0^e + \mathbf{F}_h^e + \alpha \mathbf{F}_1^e = \mathbf{0} \quad (1)$$

where  $\mathbf{A}^e$  and  $\mathbf{B}^e$  are  $(6 \times 3)$  matrices of the coefficients of the redundant unknowns  $\mathbf{X}^e$  and  $\mathbf{Y}^e$  on the meridian interfaces  $j$  and  $j+1$  respectively, listed in  $(3 \times 1)$  vectors, while  $\mathbf{C}^e$  and  $\mathbf{D}^e$  are  $(6 \times 6)$  matrices of the unknowns  $\mathbf{S}_0^e$  and  $\mathbf{S}_1^e$  on the radial interfaces  $i$  and  $i+1$  respectively, listed in  $(6 \times 1)$  vectors;  $\mathbf{F}_0^e$  is the  $(6 \times 1)$  vector of the dead loads,  $\mathbf{F}_h^e$  is the  $(6 \times 1)$  vector of the possible action of the hoop, and  $\mathbf{F}_1^e$  the  $(6 \times 1)$  vector of the live load increasing through the  $\alpha$  collapse multiplier.

It is necessary to specify that, in the problem under examination, only the unknowns  $\mathbf{S}_1$  remain on the radial faces, because the  $\mathbf{S}_0$  ones are zero on the face of the block at the top and, as regards to every other block, they coincide with the unknowns  $\mathbf{S}_1$  of the  $i+1$  face of the previous block.

## YIELD DOMAINS FOR THE GENERIC INTERFACE

With reference to a generic quadrilateral interface (Fig.6), the six stress resultants on generic radial interface  $i+1$  have to respect the yield conditions related to rocking and sliding domains; whereas, on generic interfaces  $j$  and  $j+1$  lying on meridian symmetry planes, the stress resultants only are three (the normal force and the two bending moments) and just have to respect the conditions related to rocking domain. In the following, linearized yield domains circumscribing the actual nonlinear ones are shown.

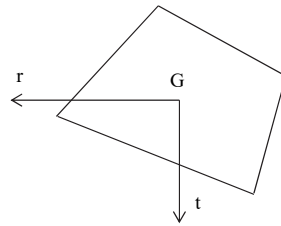


Figure 6: Generic quadrilateral interface and local reference

*Linear rocking yield domains*

For the case of unlimited compression strength, a linear yield domain was proposed in [3, 4] with reference to the quadrilateral section of Fig. 7; within a coherent kinematic mechanism, the rotation axis has to coincide with one of the four section sides, so we imposed four limit conditions:

$$d_i N_i + M_i = 0 \tag{2}$$

with  $d_i$  (Fig.7a) distance between the G centroid and the generic side  $i$  ( $i=1, 2, 3, 4$ ), and  $M_i = \mathbf{M} \cdot \mathbf{k}_i$ , being  $\mathbf{M} = M_r \mathbf{k}_r + M_t \mathbf{k}_t$  the Cartesian expression of the bending moment  $\mathbf{M}$  (Fig.7b).

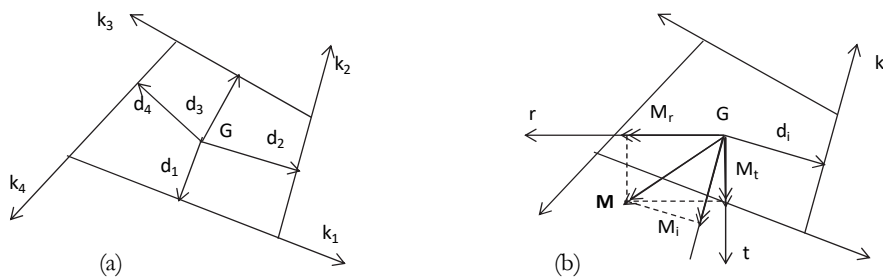


Figure 7: The quadrilateral interface. (a) Geometric aspect; (b) Mechanical aspect.

These conditions define four planes passing through the origin O of the 3D-reference ( $M_t, M_r, N$ ), that form the pyramid of Fig. 8, having cross section homothetic to the quadrilateral interface (coincident with the linear domain proposed in [18] starting by a different formulation).

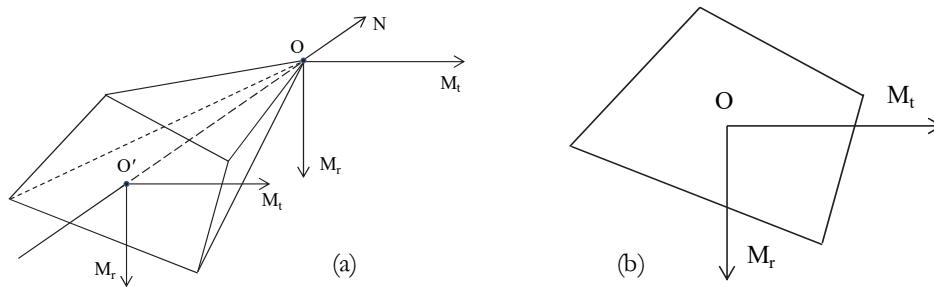


Figure 8: Yield domain. (a) The four planes through the origin O; (b) Cross section.

As the present paper only consider vertical loads, here we have assumed a limited compression strength of the masonry; in order to include a limit to the compressive stress into domain of Fig. 8, we have added four planes parallel to N-axis of the 3D-reference ( $M_t, M_r, N$ ), and four other planes forming an opposite pyramid passing through the Q point at abscissa  $N=N_0$ , being  $N_0$  the limit normal force applied in the G centroid which leads the entire section to the collapse. This linear yield domain results circumscribed to the approximate nonlinear one proposed in [18], where an additional quadratic term

on  $N$  was enclosed to take into account the limited compression strength. We note that the cross section of the two domains coincide at abscissa  $N=N_0/2$  (Fig. 9, referred to the  $(M_1, M_2, N)$  3D space, being  $M_1$  and  $M_2$  the components of  $M$  in the section principal reference).

The twelve planes are summarized by the following equations:

$$d_i N_i + M_r(k_r \cdot k_i) + M_t(k_t \cdot k_i) = 0 \quad (3)$$

$$M_r(k_r \cdot k_i) + M_t(k_t \cdot k_i) + d_i N_0 / 4 = 0 \quad (4)$$

$$-d_i N_i + M_r(k_r \cdot k_i) + M_t(k_t \cdot k_i) + d_i N_0 = 0 \quad (5)$$

being  $i$  the generic side ( $i=1, 2, 3, 4$ ).

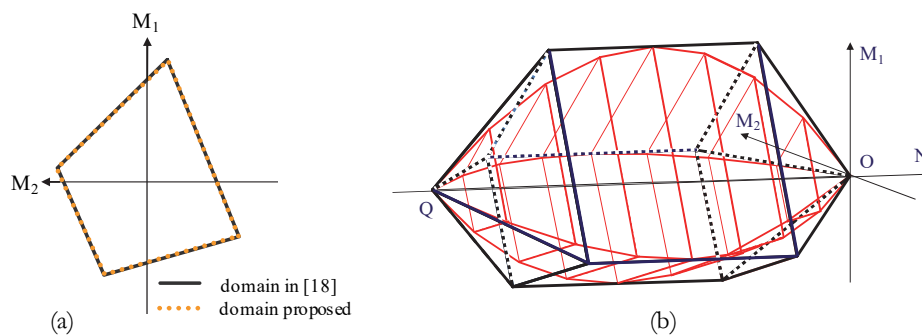


Figure 9: Yield domain for rocking in the 3D space  $(M_1, M_2, N)$ . (a) Cross section at  $N=N_0/2$ ; (b) 3D view (axonometric projection) of linearized yield domain proposed and the approximate non linear one proposed in [18].

If in the Eqns. (3)-(5) the sign ( $=$ ) is replaced with ( $\leq$ ), the conditions for  $N$ ,  $M_r$  and  $M_t$  that define the linearized yield domain are obtained.

### Linear sliding yield domains

As mentioned above, the twelve conditions (3)-(5) related to rocking domain are necessary for all the interfaces, while further conditions related to sliding domain (Fig.10) must be added about radial interfaces.

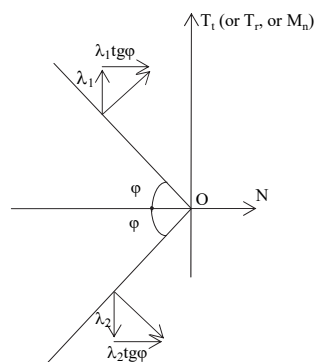


Figure 10: Yield domain for sliding.

In particular, the yield domain *normal force*  $N$  – *shear force*  $T$  is defined by a cone (Fig.11a), with axis coinciding with the  $N$ -axis has been opportunely replaced, in this first approach, by a pyramid - circumscribed to the cone - having four faces. Therefore we impose four conditions making reference to the Cartesian components  $T_t$  and  $T_r$  of  $\mathbf{T}$  shear force:



$$\tan\varphi_0 N \pm T_t \leq 0 \tag{6}$$

$$\tan\varphi_0 N \pm T_r \leq 0 \tag{7}$$

Thus, in Fig. 10,  $\varphi$  coincide with the angle of friction  $\varphi_0$ .

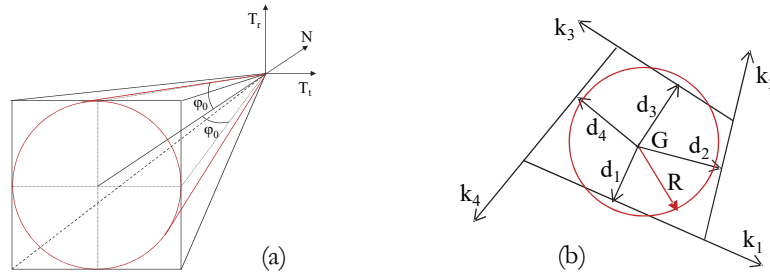


Figure 11: Yield domain for sliding. (a) Yield domain *normal force N - shear force T*; (b) Yield domain *normal force N - twisting moment \$M\_n\$*, "equivalent" circular section.

Instead, for the yield domain *normal force N - twisting moment \$M\_n\$* reference was made to an "equivalent" circular section having radius \$R\$ equal to the mean of the distances of \$G\$ by the sides of quadrilateral section (Fig.11b):

$$R = \frac{1}{4}(d_1 + d_2 + d_3 + d_4) \tag{8}$$

Therefore two conditions are imposed:

$$\frac{2}{3} R \tan\varphi_0 N \pm M_n \leq 0 \tag{9}$$

being, in the yield domain by sliding of Fig. 10,  $\tan\varphi = \frac{2}{3} R \tan\varphi_0$ .

In matrix form, the conditions on the generic meridian interface and on radial one can be expressed respectively by:

$$\mathbf{Y}^{mf} = \mathbf{D}_x^{mf} \mathbf{X}^{mf} - \mathbf{TN}^{mf} \leq \mathbf{0} \tag{10}$$

$$\mathbf{Y}^{rf} = \mathbf{D}_s^{rf} \mathbf{S}_1^{rf} - \mathbf{TN}^{rf} \leq \mathbf{0} \tag{10'}$$

where  $\mathbf{Y}^{mf}$  is a (12x1) vector,  $\mathbf{D}_x^{mf}$  is a (12x3) matrix of the coefficients of the redundant unknowns  $\mathbf{X}^{mf}$  (that is  $\mathbf{X}^{f(j)}$  or  $\mathbf{Y}^{f(j+1)}$  on the meridian faces  $j$  and  $j+1$  respectively), listed in (3x1) vector, while  $\mathbf{TN}^{mf}$  is a (12x1) vector of known terms. Moreover  $\mathbf{Y}^{rf}$  is a (18x1) vector,  $\mathbf{D}_s^{rf}$  is a (18x6) matrix of the only  $\mathbf{S}_1^{rf}$  unknowns on the radial faces  $i+1$ , listed in a (6x1) vector, while  $\mathbf{TN}^{rf}$  is a (18x1) vector of known terms.

### GOVERNING EQUATIONS OF WHOLE STRUCTURE AND ASSESSMENT OF THE COLLAPSE MULTIPLIER $\alpha$

Named  $m$  the number of balance equations for whole structure and  $n$  the number of the unknowns on the interfaces, in matrix form we have:

$$\mathbf{AX} + \mathbf{F} + \alpha \mathbf{F}_1 = \mathbf{0} \tag{11}$$

where  $\mathbf{A}$  is a ( $m \times n$ ) matrix of the coefficients of the unknowns  $\mathbf{X}$  on the interfaces, listed in the ( $n \times 1$ ) vector, while  $\mathbf{F}$  is the ( $m \times 1$ ) vector of the dead loads and of the possible actions of the hoops, and  $\mathbf{F}_1$  the ( $m \times 1$ ) vector of the live load increasing by the unknown collapse multiplier  $\alpha$ .



Moreover, named  $d$  the number of the yield domain conditions, in matrix form we have:

$$\mathbf{Y} = \mathbf{D} \mathbf{X} - \mathbf{TN} \leq \mathbf{0} \quad (12)$$

where  $\mathbf{Y}$  is a  $(dx1)$  vector,  $\mathbf{D}$  is a  $(dxn)$  matrix and finally  $\mathbf{TN}$  is a  $(dx1)$  vector of known terms.

Now the static theorem of limit analysis can be applied to evaluate the collapse multiplier  $\alpha$ , by implementing the following problem of mathematical optimization:

$$\begin{aligned} &\text{maximize } \alpha && \text{subject to:} && (13) \\ & && \mathbf{AX} + \mathbf{F} + \alpha \mathbf{F}_1 = \mathbf{0} && \text{(balance equations)} \\ & && \mathbf{Y} = \mathbf{D} \mathbf{X} - \mathbf{TN} \leq \mathbf{0} && \text{(yield domain conditions)} \\ & && \alpha \geq 0 && \text{(not negativity of } \alpha) \end{aligned}$$

being  $\mathbf{X}$  and  $\alpha$  the unknowns of the problem.

### RECONSTRUCTION OF THE COLLAPSE MECHANISM

Once the unknowns  $\alpha$  and  $\mathbf{X}$  have been defined through the static theorem of the limit analysis (paragraph 5), is possible pursue the kinematic problem to identify the corresponding collapse mechanism. The unknowns of problem are:

- $(mx1)$  vector  $\mathbf{u}$  which collects the degrees of freedom, six for every block of the discretized structure;
- $(nx1)$  vector  $\Delta$  which collects the possible displacements between the interfaces (six for every radial interface and three for every meridian one);
- $(dx1)$  vector  $\lambda$  which collects the generalized strain rates associated to the yield conditions  $\mathbf{Y}$  (Eq.12).

These unknowns are bounded by *kinematic conditions*:

$$\mathbf{A}^T \mathbf{u} = \Delta \quad (14)$$

and by the *flow rule*

$$\Delta = \mathbf{D}^T \lambda \quad (15)$$

from which, by eliminating  $\Delta$ , we obtain the *compatibility conditions*:

$$\mathbf{A}^T \mathbf{u} - \mathbf{D}^T \lambda = \mathbf{0} \quad (16)$$

being  $\mathbf{A}^T$  and  $\mathbf{D}^T$  the transposed matrices of  $\mathbf{A}$  and  $\mathbf{D}$  respectively (defined in paragraph 5).

If we denote with  $L_v = \mathbf{F}^T \mathbf{u} + \alpha \mathbf{F}_1^T \mathbf{u} + \mathbf{X}^T \Delta$  the virtual work done by the forces through the associated displacements and by the stress resultants through the mutual displacements between the interfaces, the problem of mathematical optimization is set in the following way:

$$\begin{aligned} &\text{It is imposed } L_v = 0 && \text{subject to:} && (17) \\ & && \mathbf{A}^T \mathbf{u} - \mathbf{D}^T \lambda = \mathbf{0} && \text{(compatibility conditions)} \\ & && \lambda \geq \mathbf{0} && \text{(not negativity of } \lambda) \end{aligned}$$

Once solved the problem (17), the kinematic mechanism is represented at the instant in which the collapse is reached through suitable matrices of directional cosines.



## RESULTS

The above described discrete model has been implemented by using Excel and its Solver. Although for the considered application cases has always been used a discretization in only eight macro-elements (six for the dome and two for the drum), the implemented program appears sufficiently versatile and, in addition to the mechanical characteristics, allows to define the intrados profile, the thickness variability, as well as to insert any window opening in the drum, the lantern at the top and the hoops at each level.

Once the collapse loads multiplier has been found, through the introduction of appropriate matrices of directional cosines and taking advantage of the symmetry, the program provide the collapse mechanism of a quarter of a dome, represented through axonometric and zenithal views, and a section.

In order to test the validity of the procedure, was considered a single dome with the same geometric and mechanical characteristics, and was analyzed the effect on the load-bearing capacity of the following features:

- (a) lack/presence of interlocking between the bricks at the ribs;
- (b) hoops in the case of possible failure at the ribs;
- (c) absence/presence of window openings in the drum;
- (d) drum width.

The dome examined have the following geometric and mechanical characteristics:

- the internal angular profile SA is a sixth of an acute fifth
- horizontal internal semi diameter his = 11.5 m
- thickness on top s0 = 1.5 m
- thickness at base plane of dome sI = 1.5 m
- thickness of drum sT = 1.5 ÷ 2.5 m
- drum height hT= 8 m
- height window opening hf= 6 m
- half-width window opening Lf= 2 m
- lantern radius RL = 2 m
- lantern weight on a segment of dome PL= 100 kN
- limit compressive strength  $\sigma_0 = -4000 \text{ kN/m}^2$
- friction coefficient fc= 0.75
- masonry density  $\gamma_m = 18 \text{ kN/m}^3$
- density of covering material (as overload)  $\gamma_c = 10 \text{ kN/m}^3$
- pre-tension force of a single hoop Nh = 200 kN

The numeric results (multiplier  $\alpha$ ) are summarized in the Tab. 1 and compared in Tab. 2.

Case	Failure at ribs	Lf (m)	Nh (kN)	sT (m)	$\alpha$
<b>1</b>	<b>no</b>	<b>0</b>	<b>0</b>	<b>1,5</b>	<b>24.129</b>
<b>2</b>	<b>no</b>	<b>2</b>	<b>0</b>	<b>1,5</b>	<b>14.224</b>
3	no	0	0	2,5	32.374
4	no	2	0	2,5	29.112
5	yes	0	0	1,5	7.567
6	yes	0	400	1,5	10.211
<b>7</b>	<b>yes</b>	<b>2</b>	<b>0</b>	<b>1,5</b>	<b>3.168</b>
<b>8</b>	<b>yes</b>	<b>2</b>	<b>400</b>	<b>1,5</b>	<b>7.624</b>
9	yes	0	0	2,5	17.621
10	yes	0	400	2,5	18.857
<b>11</b>	<b>yes</b>	<b>2</b>	<b>0</b>	<b>2,5</b>	<b>13.046</b>
12	yes	2	400	2,5	14.342

Table 1: Examined cases.



Features	Compared cases	Increase %	Decrease %
(a)	1-5		68.637
<b>(a)</b>	<b>2-7</b>		<b>77.73</b>
(a)	3-9		45.570
(a)	4-11		55.188
(b)	5-6	34.940	
<b>(b)</b>	<b>7-8</b>	<b>140.693</b>	
(b)	9-10	7.012	
(b)	11-12	9.936	
<b>(c)</b>	<b>1-2</b>		<b>41.049</b>
(c)	3-4		10.074
(c)	5-7		58.141
(c)	9-11		25.964
(d)	1-3	34.171	
(d)	2-4	104.672	
(d)	5-9	132.853	
<b>(d)</b>	<b>7-11</b>	<b>311.843</b>	

Table 2: Compared cases.

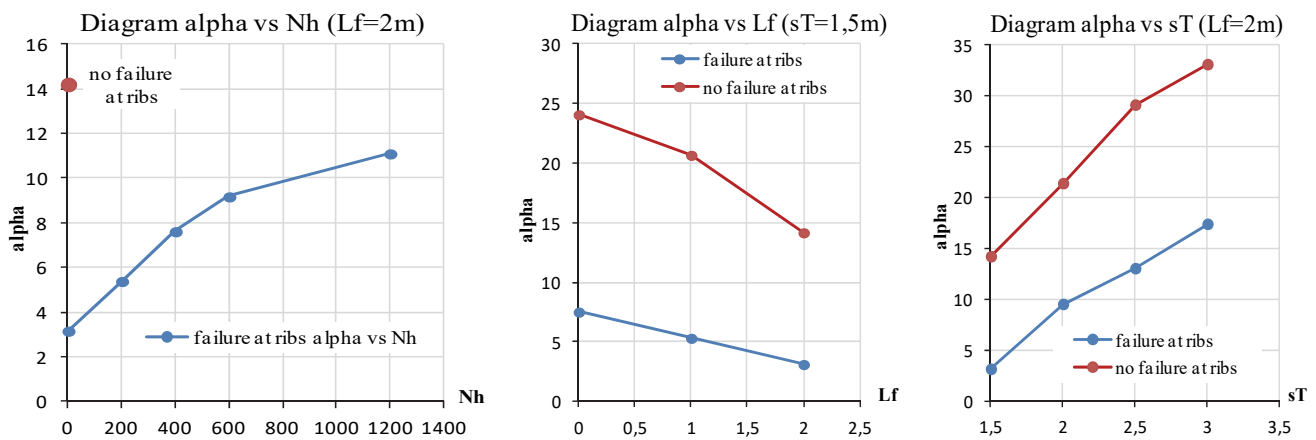


Figure 12: Variability of  $\alpha$  multiplier as a function of  $N_h$ ,  $L_f$  and  $s_T$ .

Fig. 12 shows the variability of  $\alpha$  multiplier as a function of  $N_h$ ,  $L_f$  and  $s_T$  parameters. Furthermore, some compared cases of Tab. 2 are shown in the following subparagraph 7.1 together with the relative collapse mechanisms. Finally, in subparagraph 7.2, some results obtained by examining the most famous pavilion dome in the world, that of S. Maria del Fiore by Brunelleschi in Florence, are illustrated.

*Some compared cases with relative collapse mechanisms*

We refer to compared cases shown in bold in Tab. 2. Only for practical display reasons the comparisons relating to the four features listed above with (a), (b), (c) and (d) will be illustrated below in order (c), (a), (b) and (d).

As previously mentioned, Figs. 13-17 show the collapse mechanism of a quarter of a dome, represented through axonometric and zenithal views, and a section.



Feature (c): absence/presence of window openings in the drum

With reference to the cases 1 and 2 shown in bold in Tab. 1, for the dome analyzed without failure at ribs and without windows (case 1 shown in Fig.13) the multiplier  $\alpha$  is equal to about 24, while with a window the value decreases to about 14 (case 2 shown in Fig.14).

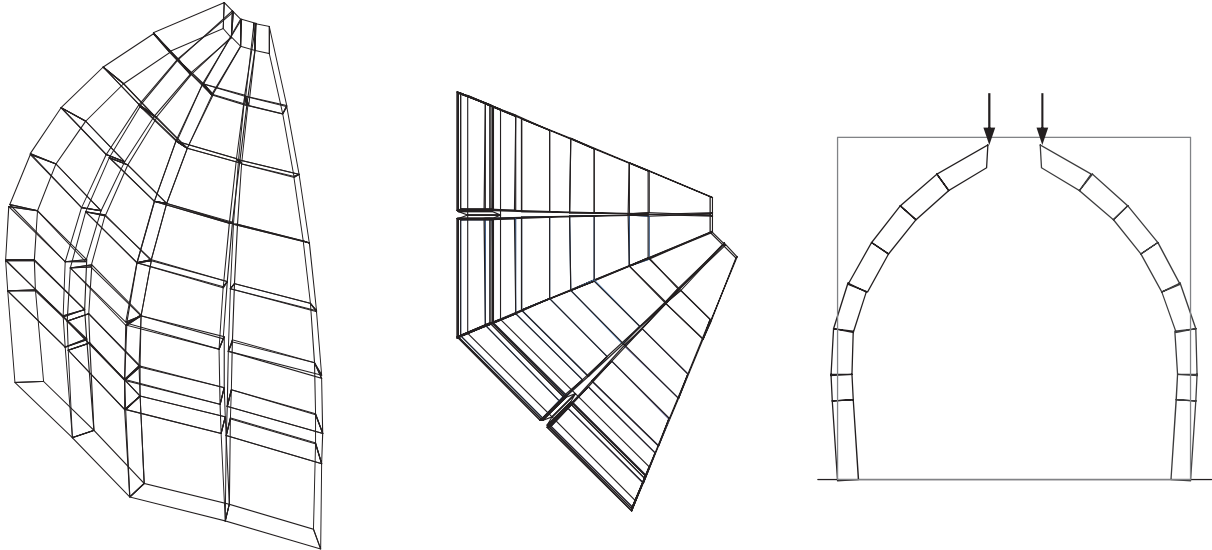


Figure 13: Collapse mechanism for case 1 (no failure at ribs /  $L_f=0$  /  $N_h=0$  /  $s^T=1.5$  / multiplier  $\alpha=24.129$ )

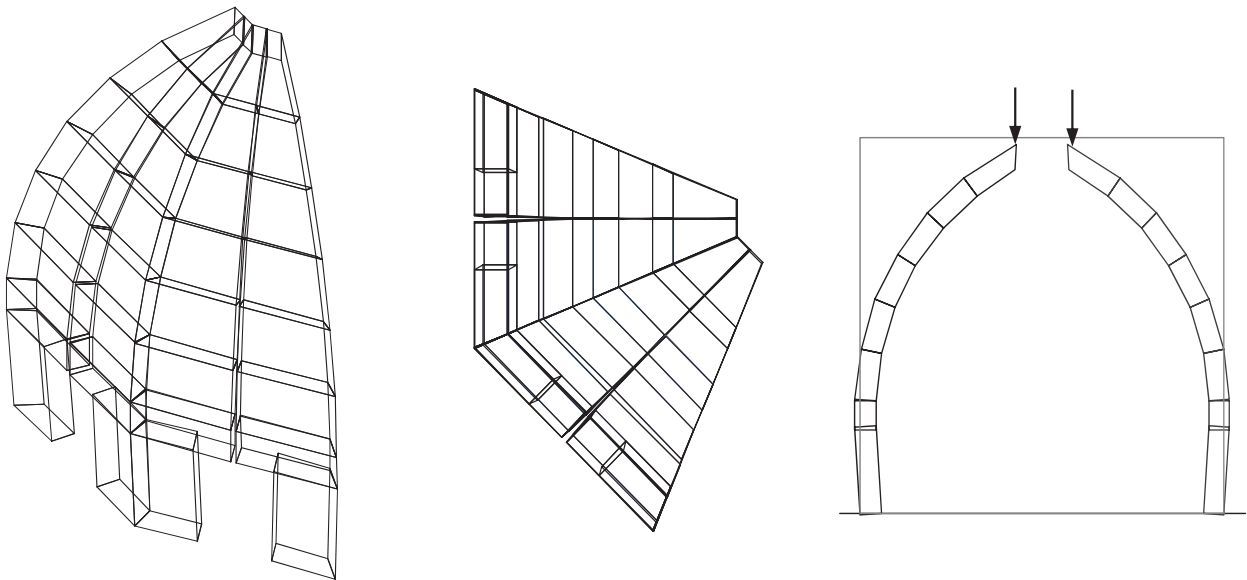


Figure 14: Collapse mechanism for case 2 (no failure at ribs /  $L_f=2$  /  $N_h=0$  /  $s^T=1.5$  / multiplier  $\alpha=14.224$ )

Feature (a): lack/presence of interlocking between the bricks at the ribs;

For the same dome with window (case 2 shown in Fig.14) in case of possible failure at ribs the multiplier value decreases from 14 to about 3 (case 7 shown in Fig.15).

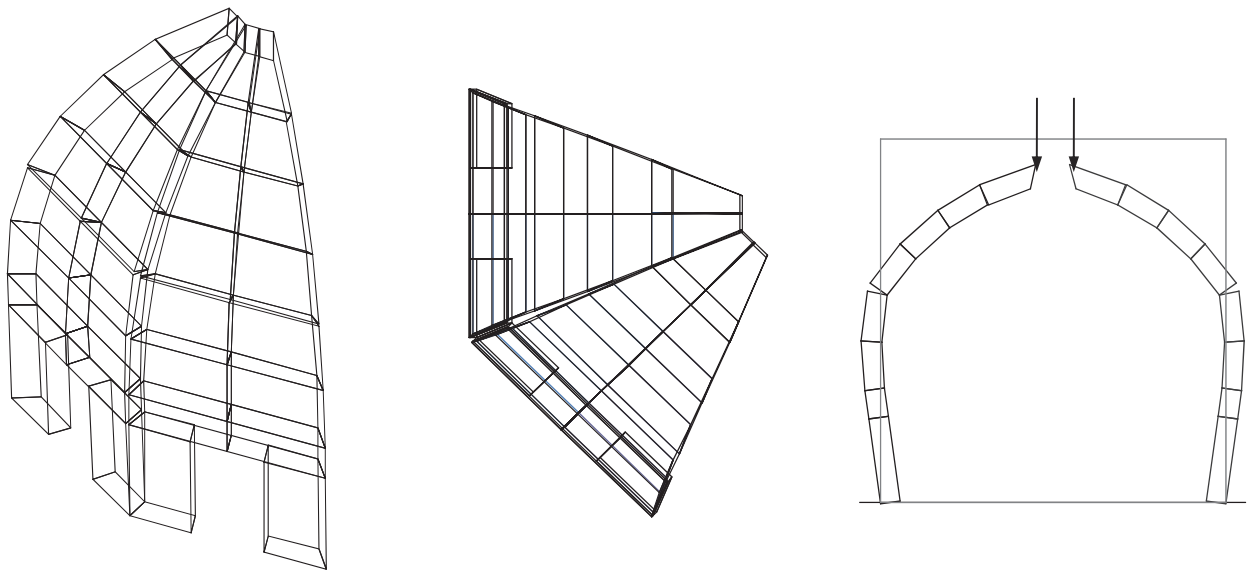


Figure 15: Collapse mechanism for case 7 (failure at ribs /  $L_f=2$  /  $N_h=0$  /  $s^T=1.5$  / multiplier  $\alpha=3.168$ )

Feature (b): hoops in the case of possible failure at the ribs;

For the same case 7 shown in Fig.15 with possible failure at ribs, if you introduce 2 hoops the  $\alpha$  value increases to about seven and half (case 8 shown in Fig.16).

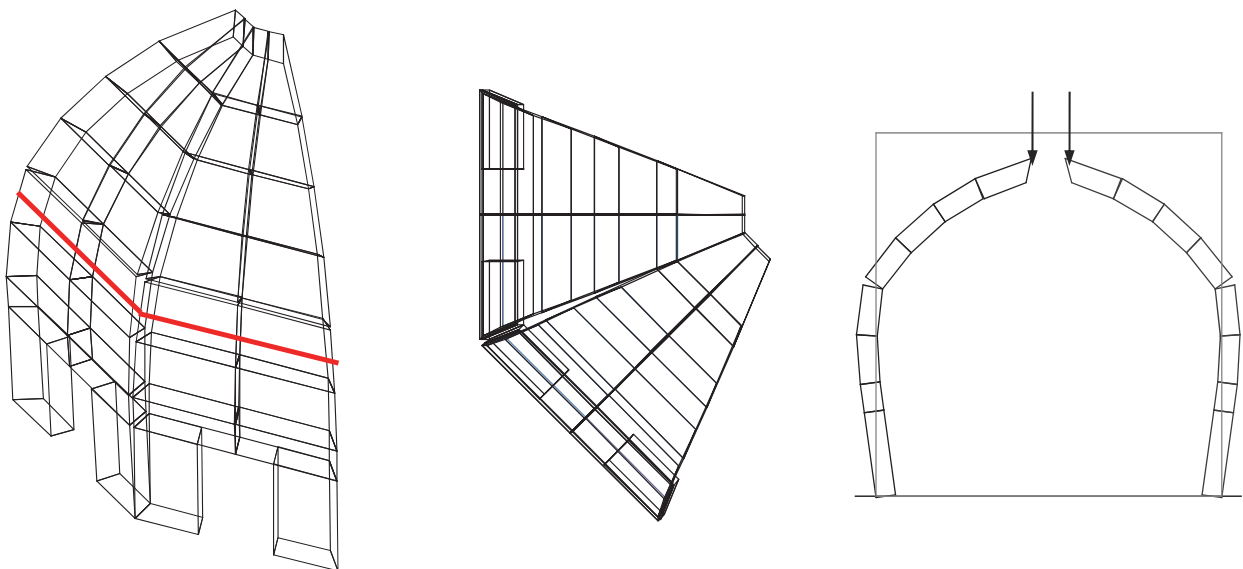


Figure 16: Collapse mechanism for case 8 (failure at ribs /  $L_f=2$  /  $N_h=400$  /  $s^T=1.5$  / multiplier  $\alpha=7.624$ )

Feature (d): drum width.

Finally, if instead of introducing the hoops (Fig.16), the thickness of the drum is increased from 1.5 to 2.5 meters, the  $\alpha$  value increases from about 3 (case 7 shown in Fig.15) to about 13 (case 11 shown in Fig.17).

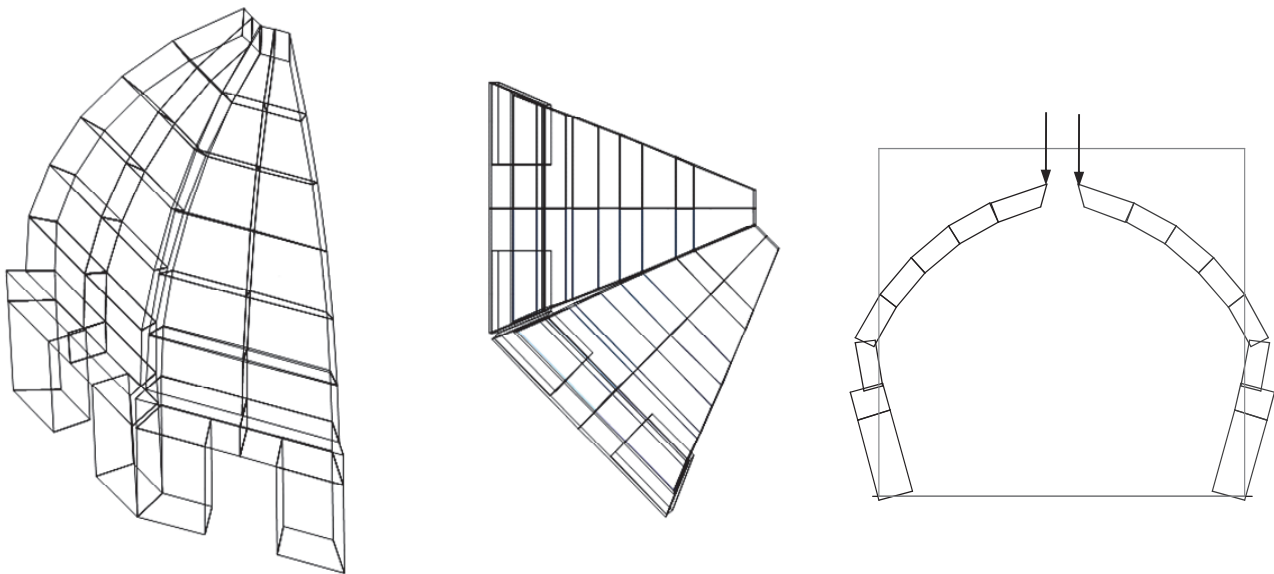


Figure 17: Collapse mechanism for case 11 (failure at ribs /  $L_f=2$  /  $N_h=0$  /  $sT=2.5$  / multiplier  $\alpha=13.046$ )

#### *The case of S. Maria del Fiore*

To validate the optimization program developed in Excel, also on a actual dome, a first approach was made to the analysis of the most famous dome on octagonal drum: the one built by Brunelleschi for the Cathedral of Florence between 1420 and 1436, of which numerous researchers have dealt [19-22].

Obviously - as has already been done by other authors who have carried out various types of analysis - it is assumed that the drum is a regular octagon, and with it also the dome; this allows us to study only one sixteenth of the dome, as for the theoretical one examined above.

Actually, compared to the theoretical model assumed, the octagonal dome shows some irregularities concerning geometry and static behavior:

- the sides have different lengths each-other,
- the drum rests alternately on four solid walls (inclined at  $45^\circ$  with respect to the axis of the nave) and on four ogival arches (two parallel to the axis of the nave and two to that of the transept), with a consequent different crack pattern, also determined from the different structural elements that surround it.

Moreover, the architectural reliefs carried out over the centuries present notable differences between them.

To overcome the uncertainties related to the dimensions of some elements that characterize the structure, we have taken the dimensions assumed by M. Como [19] using some rounding done by G. Conti [20].

In the Excel program, which for the dome (excluding the drum) provided a discretization in six elements, an further block was introduced on top, at the base of the lantern, in analogy to what was done by Como [19], while the other 30 voussoirs of its discretization have been incorporated by us, in groups of 5, into our 6 blocks. However, despite using the average value of the unit weight of the brick masonry assumed by him, we have taken into account the different unit weight of the portions of masonry made of sandstone present both in the part at the base of the dome and in the ring on top, named *serraglio*. Anyway, the weight of the dome (including the lantern) estimated by us is 29,272 t, quite close to the value reported by other scholars.

The hypothesis that, despite the octagonal form, Brunelleschi have built a rotational dome (and therefore without the use of a supporting framework), remained secret for 500 years, but in recent times shared by all the most recent scholars of masonry structures, starting by Di Pasquale [21], supports the conviction that in correspondence of the ribs there is a continuity of masonry texture, with good interlocking between the bricks. This has allowed us to introduce the assumption that in the  $(j+1)$  faces (see Fig.2) of the blocks of the analyzed segment belonging to the meridian plane passing through the rib there is no failure.

Furthermore, having the purpose of making a comparison with the pressure curve shown by Como [19], that starting from the top of the dome involves the whole upper part of the drum, 13 meters high, we had to make a second modeling. In fact, the limitation imposed by the program implemented in Excel - just two blocks to discretize the drum - led us to



adopt a different modeling of the *oculus* (circular hole). However, as for the first modeling, the same horizontal maximum width of 5.8 meters assumed in [19] as average diameter was utilized:

modeling 1 (later called Mod1). The oculus has been modeled with a hexagonal shape, but the drum is not considered in all its height, because the basic section of our calculation model was placed in the horizontal plane that cuts in half the aforementioned oculus. To this plan belong the faces (i+1) (Fig.2), i.e. those that have the smallest area and are therefore more prone to crushing failures.

modeling 2 (later called Mod2). To be able to consider the whole upper part of the drum, the oculus has been modeled with a lozenge shape having vertical axis equal to the height of the drum (13 m), and the horizontal one equal to 5.8 m. The mechanical and geometrical characteristics assumed for the dome are listed below in Tabs. 3 and 4.

Mechanical data	Values and units of measure
friction coefficient $f_c$	0.75
masonry density $\gamma_m$	18.5 kN/m <sup>3</sup>
sandstone density $\gamma_s$	25 kN/m <sup>3</sup>
density of covering material (as overload) $\gamma_c$	10 kN/m <sup>3</sup>
limit compressive strength $\sigma_0$	-4000 kN/m <sup>2</sup>
lantern weight on a segment of dome PL	469 kN

Table 3: Mechanical data of S. Maria del Fiore dome.

Geometric data	In the plane passing from ribs dimensions (m)	In the plane that cuts the sails dimensions (m)	Heights and other dimensions (m)
outer diameter	54	49.88	
internal diameter	45	41.57	
radius of arch pointed-fifth	36		
dome thickness at the base	4.5	4.15	
outside diameter of the lantern base	7	6.47	
drum thickness	5	4.6	
dome height			35.75
drum height for Mod1			7.5
height of the drum upper block for Mod1			4.6
height of the drum lower block for Mod1			2.9
drum height for Mod2			13
height of the drum upper block for Mod2			7.5
height of the drum lower block for Mod2			5.5
average diameter of the oculus			5.8

Table 4: Geometric data of S. Maria del Fiore dome.

With the program implemented in Excel, for Mod1 and Mod2, three different analyses were performed:

- (1) the classical one already applied to the theoretical dome (see previous sub-paragraph 7.1);
  - (2) a similar analysis but applied to the dome in the current state, taking into account the cracks already present;
  - (3) a comparison between the pressure curve obtained from M.Como and shown in [19] and those obtained with Mod2.
- More precisely, as regards points (1) and (2), the value of the collapse load multiplier obtained is the same, so this value can provide an indication, even if approximate, about the safety of the actual dome subject to vertical loads. On the other hand, the almost coincident values obtained with Mod2 are justified by the fact that, as for the Mod1, the failure occurs by crushing at the lower area section, corresponding to interface between the two blocks of the drum, belonging to the plane

that cuts the oculus in half. Mod2 involves a slight increase in the volume of the oculus with a consequent slight decrease in the weight of the drum blocks, and this leads to the negligible growth of the  $\alpha$  multiplier value.

Finally, with regard to point (3), for a slice of dome equal to 1/8 of the entire dome, corresponding to a single sail of the dome subjected to its own weight and to that of the lantern on top, in [19] is shown the construction of the pressure curve that, starting from the upper end of the section of the voussoir at the crown, is tangent to the intrados of the dome near the haunches, and intercepts the center of the section at the drum base (Fig.20a). Instead, still using the program implemented in Excel, which analyzes a segment equal to 1/16 of the dome, two similar pressure curves were obtained using two different objectives in the optimization problem: for the first, it was imposed that the multiplier has value zero, in compliance with the condition that the curve intercepts the center of the section at the base of the drum (Fig.20b); for the second, it was imposed that the horizontal thrust transferred from the dome to the drum assumes the value of 2000 kN, in accordance with that of 400 t estimated by Como [19] (Fig.20c).

The results of the analyses referred to in points (1) and (2) are summarized in Tab. 5 (in it the ratios  $Wc1/Wa1$  and  $Wc2/Wa2$  provide indicative coefficients on collapse safety), while the most significant collapse mechanisms are shown in Figs. 18 and 19. Instead, for the comparison referred to in point (3), the pressure curve in [19] and those obtained in this paper pursuing two different objectives are shown in Fig. 20.

dome slice analysis	Mod1 $\alpha$ multiplier	Actual weight $Wa1$ (kN)	Weight at collapse $Wc1$ (kN)	Ratio $Wc1/Wa1$	Mod2 $\alpha$ multiplier	Actual weight $Wa2$ (kN)	Weight at collapse $Wc2$ (kN)	Ratio $Wc2/Wa2$
without and with cracks	30.096	23,900	122,621	5.131	30.226	27,272	126,419	4.635

Table 5: Comparison between the values obtained with Mod1 and Mod2

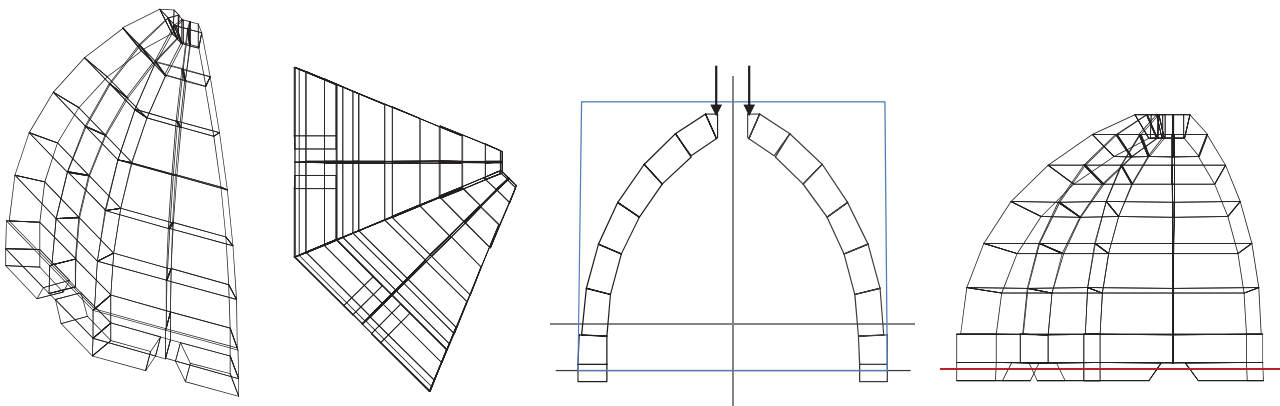


Figure 18: Collapse mechanism of S. Maria del Fiore dome (Mod1)

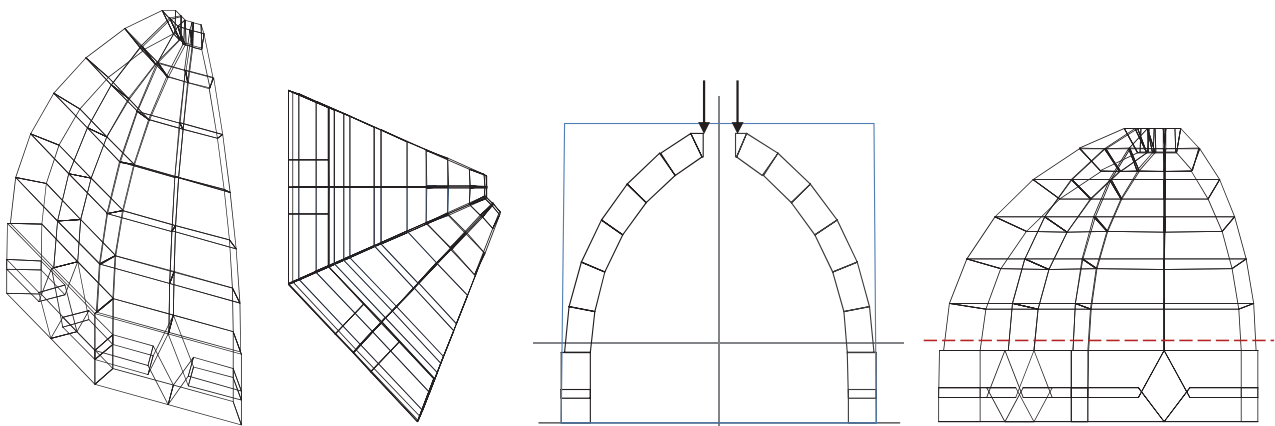


Figure 19: Collapse mechanism of S. Maria del Fiore dome (Mod2)

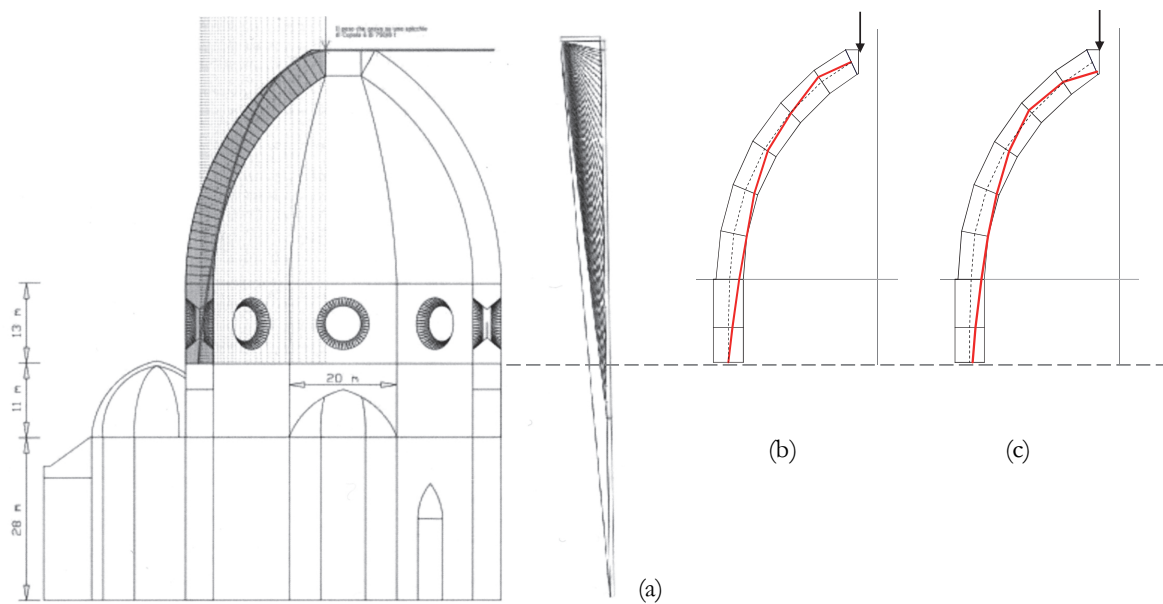


Figure 20: Comparison between our pressure curves and that of Como [19]. (a) Curve in [19]. (b) Curve obtained by imposing that it intercepts the center of the section at the drum base. (c) Curve obtained by imposing the thrust assumes the value referred in [19].

Obviously, the simplicity of the proposed model, sufficient to successfully compare the answers obtained with those expected based on the experience, does not allow a comparison to be made between the solution obtained for Brunelleschi's dome and that provided by the model illustrated in [13]. The latter, having a more dense discretization, allows the insertion of the vertical elements of the herringbone and to obtain crises due to sliding, even if with very low values of the friction coefficient.

## CONCLUSIONS

Within the framework of limit analysis applied to masonry structures, this paper has aimed at analyzing the different behavior of a pavilion dome according to the adopted construction and reinforcement technologies. By using the static theorem applied to the dome discretized in rigid macro-blocks of variable shape aligned along parallels and meridians, a mathematical model has been constructed in order to search for the load collapse multiplier, so to evaluate the degree of structural safety. Then, the associated failure mechanism is represented at the instant in which the collapse is reached. The Excel program that implement the modeling is sufficiently versatile and, in addition to the mechanical characteristics, allows to define the intrados profile, the thickness variability, as well as to insert any window opening in the drum, the lantern weight on top and hoops at each level.

The so far carried out applications, in the case of possible failure at the ribs, have shown the effectiveness of the hoops, that increases as the pre-tensioning stress increases or, alternatively, according to hoops number placed; however, for an reasonable overall force of pre-tensioning, the value of the multiplier obtained is anyway inferior to that computed in the case of a good interlocking between the bricks at the ribs. For the dome discretization into six blocks, the introduction of the hoops also seems to produce better effects if it's concentrated at the fifth ring starting from the top, rather than if distributed over several rings, for the same overall pre-tensioning force. The applications have also confirmed the effect of window openings in the drum: the value of the collapse multiplier decreases as the openings width increases.

As further developments, in addition to using the present Excel program to investigate other aspects, such as the problem of the double-shell domes and the search for the minimum thickness of the pavilion domes, the authors are implementing a Matlab program, also eventually reducing the macroblocks size in order to refine the solutions already obtained and to study also the pavilion domes under horizontal loads. Obviously, the aim is to extending these new analyses also to the dome of Santa Maria del Fiore in Florence and compare to this dome the one of Santa Maria dell'Umiltà in Pistoia, apparently similar, in which, instead, cracks at the ribs appeared already during its construction. The comparison between the two different construction methods of the two domes (with and without interlocking between the bricks at ribs), could provide confirmation that, when it is assumed that there are no cracks at ribs, it follows that the two half-segments



in contact along a rib constitute a single block. A similar assumption has been considered also by Foraboschi [22] to analyse the behaviour of the Brunelleschi dome.

## REFERENCES

- [1] Anselmi, C., De Rosa, E. and Fino, L. (2004). Limit analysis of masonry structures, Proceedings of the 4<sup>th</sup> International Seminar on Structural Analysis of Historical Constructions (edited by: C. Modena, P. B. Lourenço, P. Roca), Padova, Italy 1, pp. 545–550.
- [2] Anselmi, C., De Rosa, E., Galizia, F. and Maniello, D. (2006). Evaluation of the safety coefficient of axi-symmetric masonry domes with drum and lantern having variable profile and carrying their own weight, Proceedings of the Seventh International Masonry Conference, London, GB 5, pp. 1–6.
- [3] Anselmi, C., De Rosa, E. and Galizia, F. (2009). Evaluation of horizontal collapse for a rigid dome supported by radial masonry columns subjected to own weight. In: W.W. El-Dakhkhni, R.G. Drysdale. Proceedings of the Eleventh Canadian Masonry Symposium, Toronto, Ontario, Canada, May 31–June 3, pp. 543-550.
- [4] Anselmi, C., De Rosa, E., Galizia, F. and Maniello, D. (2009). Limit analysis of masonry domes subjected to horizontal loads, Protection of Historical Buildings - Prohitec 09 (edited by F.M. Mazzolani), Rome, Italy 2, pp. 1097-1101.
- [5] O'Dwyer, D. (1999). Funicular analysis of masonry vaults, *Comput. Struct.*, 73(1-5), pp. 187-197.
- [6] Pavlovic, M., Reccia, E. and Cecchi, A. (2016). A procedure to investigate the collapse behavior of masonry domes: some meaningful cases, *Int. J. Archit. Herit.*, 10(1), pp. 67-83.
- [7] Baggio, C., and Trovalusci, P. (2016). 3D limit analysis of roman groin vaults, Proc. 16th International Brick and Block Masonry Conference (IBMAC 2016) Padova (Italy), pp. 1023-1028.
- [8] Li, T. and Atamturktur, S. (2013). Fidelity and robustness of detailed micromodeling, simplified micromodeling, and macromodeling techniques for a masonry dome, *Journal of Performance of Constructed Facilities*, 28(3), 480-490.
- [9] Casapulla, C., Mousavian, E. and Zarghani, M. (2019). A digital tool to design structurally feasible semi-circular masonry arches composed of interlocking blocks, *Comput. Struct.*, 221, pp. 111-126.
- [10] Velilla, C., Alcayde, A., San-Antonio-Gómez, C., Montoya, F.G., Zavala, I. and Manzano-Agugliaro, F. (2019). Rampant arch and its optimum geometrical generation, *Symmetry*, 11(5), art. no. 627.
- [11] Olmati, P., Gkoumas, K. and Bontempi, F. (2019). Simplified FEM modelling for the collapse assessment of a masonry vault, *Frattura ed Integrità Strutturale*, 13(47), pp. 141-149.
- [12] Simon, J. and Bagi, K. (2016). Discrete element analysis of the minimum thickness of oval masonry domes, *Int. J. Archit. Herit.*, 10(4), pp. 457-475.
- [13] Beatini, V., Royer-Carfagni, G. e Tasora, A. (2019). A non-smooth-contact-dynamics analysis of Brunelleschi's cupola: an octagonal vault or a circular dome? *Meccanica*, 54 (3), pp. 525-547.
- [14] Lourenço, P.B. e Ramos, L.F. (2004). Characterization of cyclic behavior of dry masonry joints, *Journal of Structural Engineering*, 130(5), pp. 779-786.
- [15] Casapulla, C. and Portioli, F. (2016). Experimental tests on the limit states of dry-jointed tuff blocks, *Materials and Structures*, 49(3), pp. 751-767.
- [16] Vasconcelos, G. and Lourenço, P.B. (2009). Experimental characterization of stone masonry in shear and compression, *Construction and Building Materials*, 23(11), pp. 3337-3345.
- [17] Lee, H.S., Park, Y.J., Cho, T.F. and You, K.H. (2001). Influence of asperity degradation on the mechanical behaviour of rough rock joints under cyclic shear loading, *International Journal of Rock Mechanics and Mining Sciences*, 38(7), pp. 967-980.
- [18] Orduña, A. and Lourenço, P. (2005). Three-dimensional limit analysis of rigid blocks assemblages. Part I: Torsion failure on frictional interfaces and limit analysis formulation, *International Journal of Solids and Structures*, 42 (18-19), pp. 5140-5160.
- [19] Como, M. (2017). *Statics of Historic Masonry Constructions*, Third Edition, Springer, 4.11, pp. 242-271.
- [20] Conti, G. (2014). La matematica nella Cupola di Santa Maria del Fiore a Firenze, in *Ithaca: Viaggio nella Scienza*, n. 4, anno 2014 - Arte e Scienza, pp. 5-11.
- [21] Di Pasquale, S. (2002). *Brunelleschi. La costruzione della cupola di Santa Maria del Fiore*. Marsilio, Venice.
- [22] Foraboschi, P. (2014). Resisting system and failure modes of masonry domes, *Engineering Failure Analysis* 44, Elsevier Ltd., pp. 315–337.